Recent Progress in Liquid Crystal THz Optics

Ci-Ling Pan and Ru-Pin Pan*
Department of Photonics and Institute of Electro-Optic Engineering
Department of Electrophysics*
National Chiao Tung University 1001 Ta-Hsueh Rd., Hsinchu, Taiwan 30010, R.O.C.
Contact: clpan@faculty.nctu.edu.tw, rpchao@mail.nctu.edu.tw

ABSTRACT

Recently, there have been increasing interests in the study of liquid-crystal-based devices for application in the sub-millimeter wave or THz frequency range. In this paper, we present recent progress in liquid crystal THz optics from our group. Using time-domain THz spectroscopy, we have determined the complex indices of refraction of nematic liquid crystals, 5CB, PCH5 and E7 from 0.2 to beyond 1 THz. Significantly, the birefringence of 5CB and E7 are found to be as large as 0.2 at THz frequencies, while the absorption is negligible. Electrical-field and magnetic-field-controlled birefringence in LC were also investigated. A tunable room-temperature THz phase shifter using magnetic-field-controlled birefringence in nematic 5CB gives a phase shift as large as 108° at 1.0 THz. Phase shift exceeding 360° at 1 THz, an important milestone, was realized by using a sandwiched LC (E7, Merck) cell as thick as 3 mm. The magnetically tuned LC phase shifter served as key components in a two-element tunable LC Lyot filter. The tuning range of the filter is from 0.388 to 0.564 THz or a fractional tuning range of ~ 40%. Our work clearly demonstrates the potential of liquid crystal devices for THz applications. Finally, we will present initial works on control of enhanced THz transmission through a metallic hole array with nematic liquid crystals. Our work clearly demonstrates the potential of liquid crystal devices for THz applications.

Keywords: THz, Liquid-crystal devices, far Infrared, phase shifters, wave plate, Lyot filter

1. INTRODUCTION

In recent years, remarkable progress has been made in Terahertz (THz) photonics. With the development of solid-state femtosecond lasers and advanced optoelectronic THz-devices, a new era of fundamental and applied THz science is opening up. THz studies ranging from investigations of ultrafast dynamics in materials to medical, environmental sensing and imaging are actively explored.[1-3] For these and future applications in THz communication and surveillance, quasi-optic components such as phase shifters, modulators, attenuators and polarizers are indispensable. The birefringence of liquid crystals (LC's) is well known and extensively utilized for the manipulation of optical radiation in the visible and near-infrared range. In this paper, we present recent progress in liquid crystal THz optics from our group. In Sec. 2, we describe measurements of the complex indices of refraction of several nematic liquid crystals in the far infrared or THz frequency range. Several THz photonic devices with liquid-crystal-enabled functionalities are described in the following sections.

2. THZ BIREFRINGENCE AND OPTICAL CONSTANTS OF LIQUID CRYSTALS

One of the key parameters of the LCs is its complex refractive indices or optical constants. In the visible range, the optical constants of LCs have been extensively investigated.[4-5] In the infrared range, the refractive indices and other optical properties of LCs have also been reported.[6] In the millimeter wave range, Lim et al.[7] first showed that many LCs have comparatively large birefringence with approximate values in the of 0.1-0.18 range at 30 GHz. Further, the birefringence of LCs varied only slightly in the 15-94 GHz range. Nose et al.[8] reported the refractive indices and transmission losses for some nematic LCs, including 4, 4'-n-pentylcyanobiphenyl (5CB), have been measured by at three discrete wavelengths (118, 215, and 435 μm). The birefringence of 4-($trans$-4'-pentylcyclohexyl)-benzonitrile (PCH5) in the 0.1 to 0.8 THz range (~0.01), on the other hand, were found to be much smaller than those in the visible range (~0.12).[9]

We have measured the optical constants of 5CB, E7 (both from Merck) and PCH5 (Aldrich) using the method of THz time-domain spectroscopy. The test cell was constructed as a double-cell with a liquid crystal cell and an empty reference cell side by side. Optical-quality fused silica windows were used as substrates. The thickness of the LCs was controlled by mylar spacers with a nominal cell thickness between 50 and 120 μm. Homogeneous alignment of the nematic LC was achieved by the rubbing process. The temperature of the sample cell was regulated within ± 0.1°C. Our THz time-domain spectroscopy (THz-TDS) experimental setup is similar to the conventional THz system and has been described in detail elsewhere.[10,11] Briefly, a mode-locked Ti:Sapphire laser (λ = 800 nm) with 400 mW average output power generates ~35 fs pulses at a repetition rate of 80 MHz. The laser beam is divided into two beams, a pump and a probe. A large-aperture photoconducting antenna is used as a THz transmitter in our THz spectrometer. The transmitter consists of an As$^+$ implanted GaAs wafer with two electrodes separated by about 2 mm, on which AuGe is deposited. The two electrodes are biased with about 800 V.[12] The pump beam illuminates the area between the two electrodes with focused ultrashort laser pulses produces synchronous bursts of THz wave. The THz wave is collimated and focused on the sample by a pair of off-axis paraboloidal mirrors. The transmitted THz wave through the sample is collimated and focused again on a detector by a second pair of off-axis paraboloidal mirrors. A 2-mm-thick (110) ZnTe crystal is used in an electro-optic sampling setup for the detection of the THz wave.

A LC sample of thickness L, referred as 2, is placed between two media 1 and 3. The terahertz wave goes through the sample from medium 1 to medium 3. Assuming that a plane wave of THz wave, the spectral component at angular frequency of the electric field of the terahertz wave transmitted through the sample can be written as:

$$E_{sample}(\omega) = T_{12}(\omega)P_2(\omega,L)T_{23}(\omega) \cdot \sum_{k=0}^{\infty}\{R_{23}(\omega)P_2^{\,2}(\omega,L)R_{21}(\omega)\}^k \cdot E(\omega) \cdot \tag{1}$$

where $E(\omega)$ is the incident electric field of the terahertz wave, $R_{ij}(\omega) = \dfrac{(n_i - n_j)}{(n_i + n_j)}$ (reflection coefficient at the i–j

interface), $T_{ij}(\omega) = \dfrac{2n_i}{(n_i + n_j)}$ (transmission coefficient from medium i to medium j), and $P_i(\omega,d) = \exp(-i\,n_i\omega d/c)$

(propagation coefficient in medium i over a distance d) with $n_i(\omega) = n_i - i\kappa_i$ being the complex refractive index of

medium i which depends on the angular frequency ω. The spectral component of the electric field of the terahertz wave transmitted without the sample is given by

$$E_{ref}(\omega) = T_{1air}(\omega)P_{air}(\omega,L)T_{air3}(\omega) \cdot \sum_{k=0}^{\infty}\{R_{air3}(\omega)P_{air}^{\,2}(\omega,L)R_{air1}(\omega)\}^k \cdot E(\omega) \cdot \tag{2}$$

The complex transmission coefficient $T(\omega)$ of the sample is obtained by dividing the signal E_{sample} recorded with the sample by E_{ref} recorded without the sample

$$T(\omega) = \dfrac{E_{sample}(\omega)}{E_{ref}(\omega)} \cdot \tag{3}$$

In the case of the characterization of thin liquid crystal cell made by a modification of the fused silica surface, the refractive index of the fused silica is used to replace of n_1 and n_3.

A reference of the temporal THz waveform was first obtained by introducing a vacant cell between the THz transmitter and the receiver. Subsequently, the vacant cell was replaced by the filled cell and a second set of waveform was taken. Since a nematic LC can be viewed as a uniaxial crystal, the information for n_e and n_o of LC can be obtained by rotating the cell to adjust the director of LC being parallel and perpendicular to the polarization direction of THz wave, respectively. In Fig. 1 (a), the THz-band extraordinary and ordinary indices of refraction of 5CB at 25°C are shown. Clearly, a slow and monotonic increasing trend is evident for both n_e and n_o. In the 0.2 to 0.8 THz range, n_e increases from 1.7 to 1.96, while n_o varies from 1.55 to 1.75. The birefringence of 5CB, $\Delta n = n_e - n_o$, is thus as high as 0.15 to 0.21. In comparison, the birefringence for 5CB in the visible region varied from 0.11 to 0.20 depending on the temperature and wavelength. Figure 1(b) illustrates the imaginary indices of refraction of 5CB, k_e and k_o, in the same frequency range. These are in general of the order of 0.1 or less. No resonance was detected.

The corresponding results for PCH5 at room temperature are shown in Fig. 2(a) and (b). We also observed a slow and monotonic increasing trend for both n_e and n_o of PCH5. In the 0.2 to 0.8 THz range, n_e increases from 1.42 to 1.56, while n_o varies from 1.42 to 1.50. The birefringence of PCH5, $\Delta n = n_e - n_o$, is thus in the range from 0.01 to 0.08. This is considerably smaller than the birefringence for PCH5 in the visible region, which varies from 0.12 to 0.135 depending on the temperature and wavelength. In Fig. 2(b), we have plotted the imaginary indices of refraction

of PCH5, k_e and k_o, in the same frequency range. These are in general of the order of 0.1 or less.   Again, no resonance was detected.

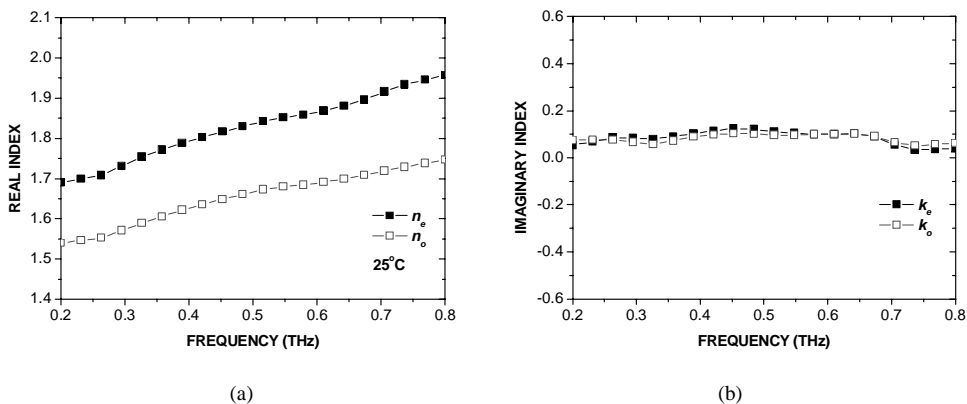(a)   (b)

Fig. 1(a) Extraordinary and ordinary indices of refraction of the LC, 5CB, is shown as a function of frequency from 0.2 to 0.8 THz. Fig. 2(b) shows the imaginary indices of refraction of 5CB in the same frequency range.
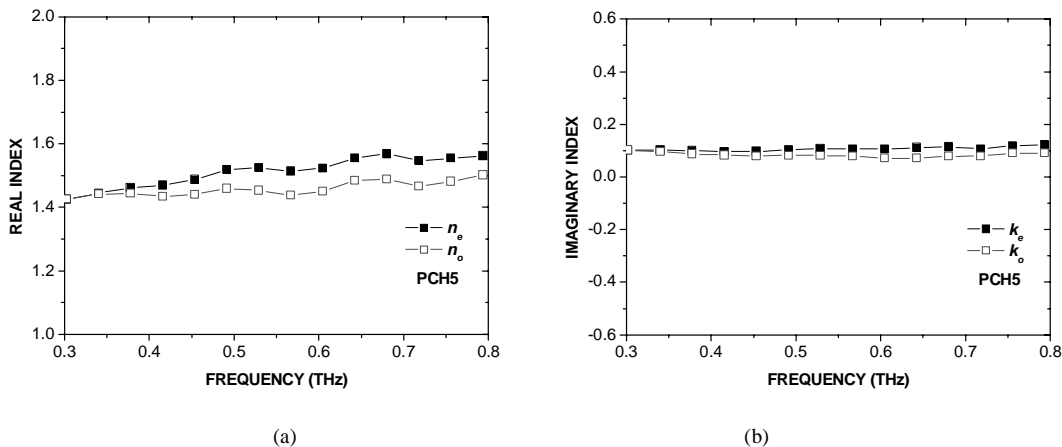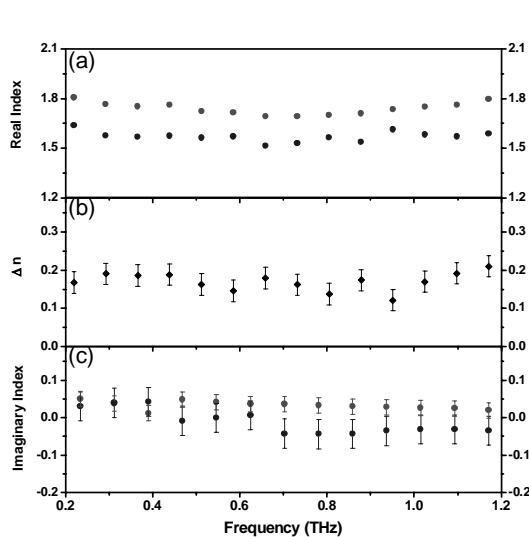

(a)   (b)

Fig. 2(a) Extraordinary and ordinary indices of refraction of the LC, PCH5, is shown as a function of frequency from 0.2 to 0.8 THz. Fig. 2(b) shows the imaginary indices of refraction of PCH5 in the same frequency range.

In Fig. 3(a), the THz–band extraordinary and ordinary refractive indices of E7 are shown. Clearly, E7 exhibits a positive birefringence ($n_e > n_o$), which is consistent with that in the visible range.   There is no sharp resonance in the 0.2-1.2 THz range, in which n_e varies from 1.69 to 1.80, while n_o varies from 1.51 to 1.63. The birefringence of E7 is thus 0.12 to 0.21 for the same frequency range (see Fig. 3 (b)). This is comparable to that of 5CB and much larger than that of PCH5 ($\Delta n \sim 0.08$).   The corresponding imaginary indices of E7 are relatively small (< 0.04, see Fig. 3(c)). That is, the extinction coefficient of E7 is less than 2 cm^{-1}. Thus E7 exhibit high birefringence, small losses and broad nematic temperature range, which are attractive for applications such as phase shifting.

Fig. 3 The room-temperature (a) extraordinary (red circles) and ordinary (blue circles) refractive indices, (b) birefringence, and (c) imaginary extraordinary (blue circles) and ordinary (red circles) refractive indices of E7 are shown as a function of frequency.

3. MAGNETICALLY TUNED THz PHASE SHIFTER

By using magnetically controlled birefringence in a 5CB cell with nominal thickness of 1.5 mm, we were able to achieve a maximum phase shift of 141⁰ at 1.025 THz.[13]   The alignment of the LC layer becomes increasingly difficult with thicker cells. Phase shift exceeding 360° at 1 THz, an important milestone, was realized by using a sandwiched LC (E7, Merck) cell as thick as 3 mm.[14]
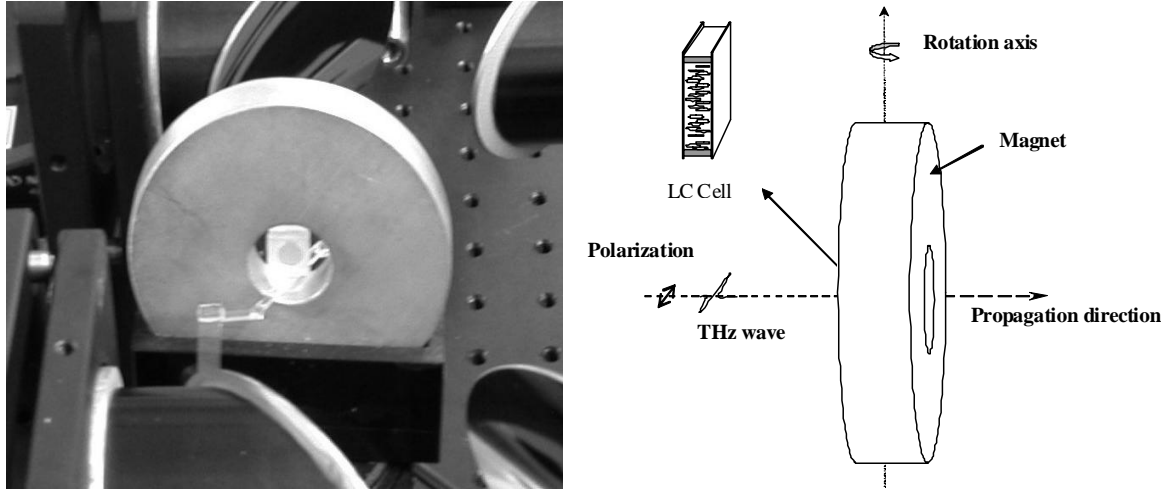

Fig.4 A photograph and the schematic diagram of the LC THz phase shifter..

The tunable THz LC Phase shifter consists of a homeotropically aligned LC cell and a rotary magnet as shown in Fig. 4. Three fused silica plates are employed for the sandwiched cell. The two compartments of the cell are filled with a common LC, E7. Teflon spacers are used for controlling the thickness of LC layers to 1.5 mm each. We employ an Nd-Fe-B sintered magnet on a rotation stage, which provides a tunable magnetic field for tuning the phase shift of the THz wave. We define the magnetic inclination angle, θ, as the angle between the magnetic field and the propagation direction. The effective refractive index of LC changes with the LC molecular orientation, which is controlled by the angle θ. The phase shift, δ(θ), due to magnetically controlled birefringence is given by

$$\delta(\theta) = \int_0^L \frac{2\pi f}{c} \Delta n_{eff}(\theta, z) dz \,, \tag{4}$$

where L is the thickness of LC layer, Δn_{eff} is the change of effective birefringence, f is the frequency of the THz waves and c is the speed of light in vacuum.

If the magnetic field is large enough such that the LC molecules are reoriented parallel to the magnetic field. The phase shift, δ(θ), in Eq.(4) can then be re-written as

$$\delta(\theta) = 2\pi L \frac{f}{c} \left\{ \left[\frac{\cos^2(\theta)}{n_o^2} + \frac{\sin^2(\theta)}{n_e^2} \right]^{-\frac{1}{2}} - n_o \right\}, \tag{5}$$

where n_o and n_e are the ordinary and extra-ordinary refractive indices of the LC. The theoretical phase shift can be calculated if we know the n_o and n_e of LC and the thickness of the LC layer.

The temporal THz profiles passing through the LC phase shifter at various magnetic inclination angles (θ = 0°, 30° and 50°) are shown in Fig. 5(a). The spectrum of the THz signal at θ = 0° is shown in the inset. The total scan range for the time delay was 12 ps, although only the data from 1 to 8.3 ps are shown. The transmitted THz waves show obviously longer time delay for larger angle, θ. The THz field amplitudes increase with θ for θ < 43°. This can be explained by the increasing transmittance at the quartz-LC interface according to the Fresnel equations. The ordinary

and extraordinary refractive indices of E7 are 1.57 and 1.76, respectively, at 1 THz. With increasing θ, the effective refractive index of LC will rise from 1.57 to 1.76 and become closer to the refractive index of quartz substrate, which is 1.95. The transmitted field amplitudes will then increase according to Fresnel equations. The THz field amplitudes decrease for θ > 43° due to partial blocking of the THz wave by the magnet. The deduced phase shifts of the phase shifters are plotted as a function of the magnetic inclination angle in Fig. 5 for 0.49 and 1.025 THz waves. The maximum phase shift achieved was 368° at 1.025 THz and θ = 54°. The theoretical predictions are plotted as the solid curves in Fig. 5(b). They show good agreements with the measured results.
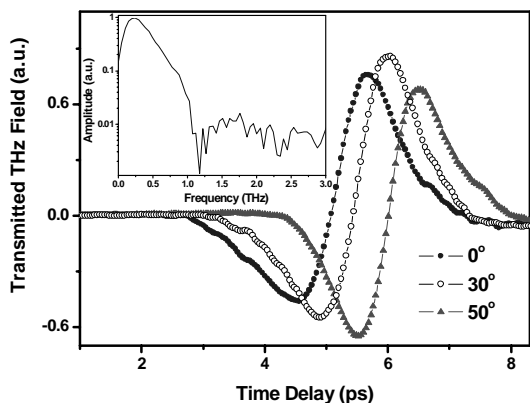

Fig. 5(a). The measured THz waveforms transmitted through the LC phase shifter at various magnetic inclination angles. The inset shows the spectrum of the THz signal.
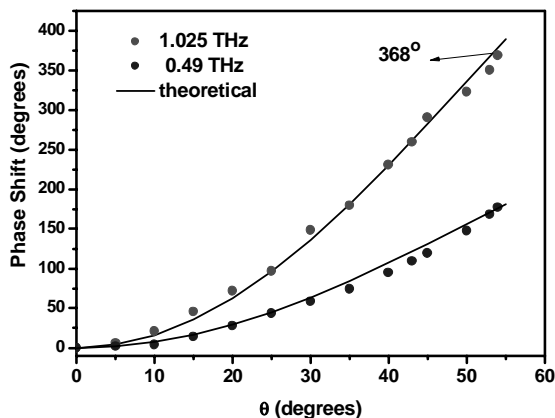

Fig. 5(b) The phase shift of the THz waves versus the magnetic inclination angle. The solid curves are theoretical predictions. The open and solid circles are experimentally measured phase shift at 0.49 and 1.025 THz.
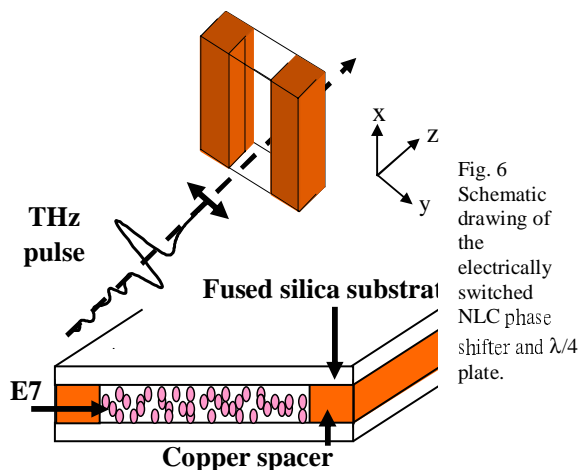
4. ELECTRICALLY TUNED THz LC PHASE SHIFTER

Fig. 6 Schematic drawing of the electrically switched NLC phase shifter and λ/4 plate.

Electrically controlled phase shifters are deemed desirable for many applications. In our previous attempt of an LC-based phase shifter, a maximum phase shift of 4.07° was achieved at 1.07 THz when the interaction length was 38.6 μm in the homogeneously aligned NLC cell. The driving voltage and corresponding field were 177 V and 589 V/cm, respectively.[15] Recently, we report an electrically tunable phase shifts beyond 90° at 1 THz in a homeotropically aligned NLC cell. The operation of the device as a THz quarter-wave (λ/4) plate is verified. The experimental results are in good agreement with calculations using the continuum theory of the NLC.

schematic of the experimental setup is shown in Fig. 6. The key element is a homeotropically aligned nematic liquid crystal (E7 by Merck) cell. The thickness of the E7 layer is 570 μm. Copper pieces (purity 99.94%) were used as spacers and electrodes. The copper pieces were parallel to each other and separated by 11.9±0.3 mm. With positive dielectric anisotropy, the E7 molecules in the bulk of cell will be reoriented toward the applied electric field once the applied bias is increased beyond the threshold voltage (the Fréedericksz transition[16]),

$$V_{th} = \pi \frac{L}{d} \left(\frac{k_3}{\varepsilon_a \varepsilon_o} \right)^{\frac{1}{2}},$$ (6)

where L is the distance between two electrodes, d is thickness of the NLC layer, k_3, $\varepsilon_a = \varepsilon_\parallel - \varepsilon_\perp$ and ε_o are the bend elastic constant, dielectric anisotropy, and electric permittivity of free space, respectively. For our device, we calculated that $V_{th} = 24.5$ V (rms), with L=11.9 mm, d=570 μm, k_3=17.1×10^{-12} N, ε_a=13.8 (from Merck). For $V > V_{th}$ the angle θ at any point z in the cell can be computed using the relation,[17]

$$\frac{z}{d} = \frac{V_{th}}{\pi V} \int_0^\theta \left(\frac{1 + q \sin^2 \theta}{\sin^2 \theta_m - \sin^2 \theta} \right)^{\frac{1}{2}} d\theta,$$ (7)

where $q = (k_1 - k_3)/k_3$, and k_1 (= 11.1×10^{-12} N for E7) is the splay elastic constant of NLC. The angle θ_m is the maximum reorientation angle located at $z = d/2$. It is related to V/V_{th} by

$$\frac{V}{V_{th}} = \frac{2}{\pi} \int_0^{\theta_m} \left(\frac{1 + q \sin^2 \theta}{\sin^2 \theta_m - \sin^2 \theta} \right)^{\frac{1}{2}} d\theta.$$ (8)

Equations (7) and (8) allow us to calculate the profile of molecular orientation in the cell for a given applied voltage.
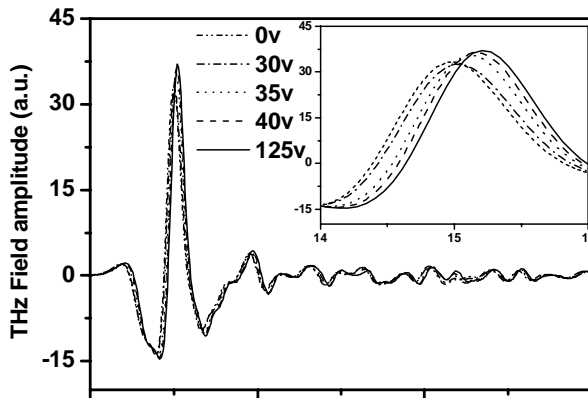

Fig. 7 The temporal waveforms of the THz pulse transmitted through the E7 cell at various applied voltages. The inset is the close-up from 14 to 16 ps.

The temporal waveforms of the THz pulse transmitted through the LC cell for various driving voltages are shown in Fig. 7. An enlarged view is shown in the inset of Fig. 7. Increasing the applied voltage, the effective index of E7 will rise from 1.62 (n_o) to 1.79 (n_e).

The transmitted THz spectra are deduced from the temporal profiles of the THz pulse with fast Fourier transform (FFT) algorithms and spectral phase shifts are determined.

Figure 8(a) shows the phase shifts as a function of driving voltage. The curves are theoretical prediction and in good agreements with the experiments. A maximum phase shift of 93.7° was achieved at 1.00 THz when the LC cell was driven at 125 V (rms). The corresponding field is 105 V/cm. The theoretically predicted phase shift was 101.75°. The threshold voltage and the corresponding field were found to be 27 V and 22.6 V/cm, respectively, also in reasonable agreement with the theoretically predicted value, 24.5 V (rms).

According to Eq. (4), larger phase shift is expected at higher frequency. This is confirmed in Fig. 8(b), in which we plot the phase shifts from 0.20 to 1.00 THz by varying the driving voltages. For a given voltage, the measured phase shift varied linearly with frequency, with a slope of ~ 89.6 degrees/THz at 125 V (rms).

To confirm that the present device can be used as a λ/4 plate, we also recorded the transmittance through the device as it was rotated with angle ϕ about the axis of propagation (Fig. 9(a)). The results (solid circles) show clearly the squared sinusoidal law dependence for the transmittance and the correct period for a λ/4 plate. The transmittance of an ideal λ/4 plate, $1 - \frac{1}{2}\sin^2(2\phi)$, is also plotted as the solid curve, which fits the experimental data without any adjustable parameter.

The error bar is due to Ti: sapphire laser power fluctuation and possibly scattering losses by the THz beam propagating through the NLC layer. The latter mechanism is currently under investigation.

The dynamics of the cell is determined by its viscosity and geometry of the cell. For our device, the $1/e$ switching-off time[17] is $\tau_{off} = \frac{\gamma d^2}{V_{th}^2 \varepsilon_a \varepsilon_0}$, where γ is the rotational viscosity. With a typical value of 0.1 Pa·s for γ,[18] we estimate that τ_{off}

~170 sec. Experimentally, we determined the switching-off time by turning off the driving voltage while monitoring the

change in the value of the transmitted THz waveform at a fixed delay of the gating optical pulse and obtained $\tau_{off} \sim 190$ sec. This is shown in Fig. 9(b)
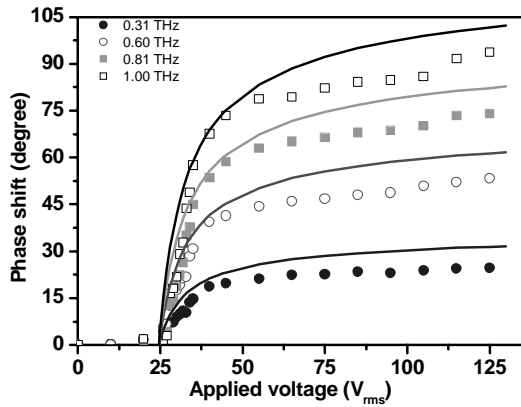

Fig. 8 (a) The phase shift as a function of driving voltage for four frequencies. The solid curves are from the theoretical prediction.
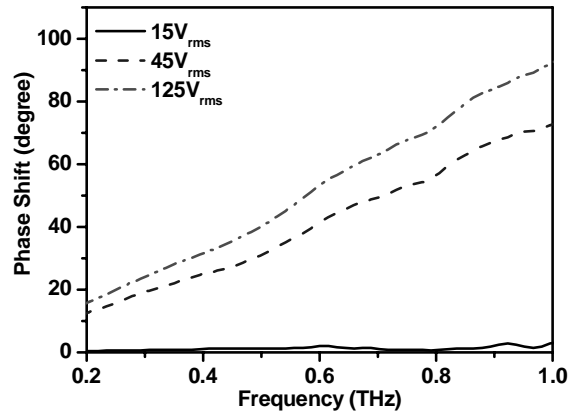
Fig. 8 (b) The phase shift from 0.20 to 1.00 THz for several driving voltages of the LC cell.
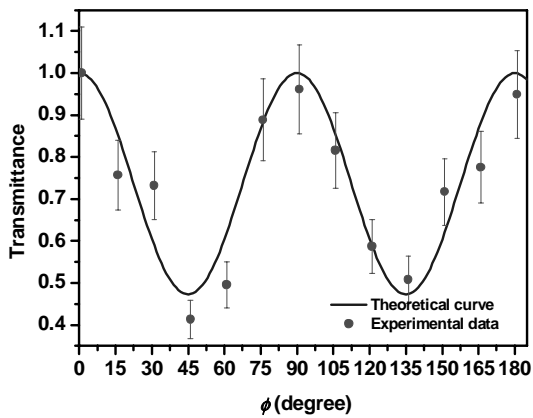

Fig. 9(a) Transmittance of the device as it was rotated about the THz beam propagation axis. The solid curve is the transmittance for an ideal $\lambda/4$ plate.
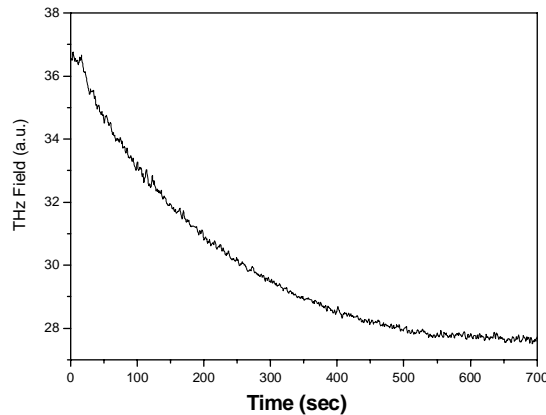
Fig. 9(b) Switching-off behavior of the electrically tunable THz phase shifter

5. TUNABLE THz LYOT FILTER

The Lyot filter[19], a prototype of birefringent filters widely employed in the visible and near infrared, is based on interference of polarized light by means of a stack of birefringent elements with their optical axes rotated with respect to each other. In the following, we describe the construction and characteristics of tunable THz Lyot filter based on magnetically controlled retardation in LC.[20]

The LC-based Lyot filter has two elements, A and B, which are separated by a linear polarizer (Fig. 10) Each element consists of a fixed retarder (FR) and a tunable retarder (TR). The FR consists of a pair of permanent magnets sandwiching a homogeneously aligned LC cell. Sufficiently large magnetic field is required for stable homogeneous alignment of LC molecules in the thick LC cell (inset (a) of Fig.10 and Fig. 4). The homogeneous cells in FR_A and FR_B supply fixed phase retardations, Γ_A and Γ_B, for THz waves. The tunable retarders, TR_A and TR_B (inset (b) of Fig. 10) are

of our previous design (see Sec. 3), i.e., a homeotropically aligned LC cell at the center of the rotatable magnet. TR_A and TR_B are used to achieve the desired variable phase retardation, $\Delta\Gamma_A$ and $\Delta\Gamma_B$.
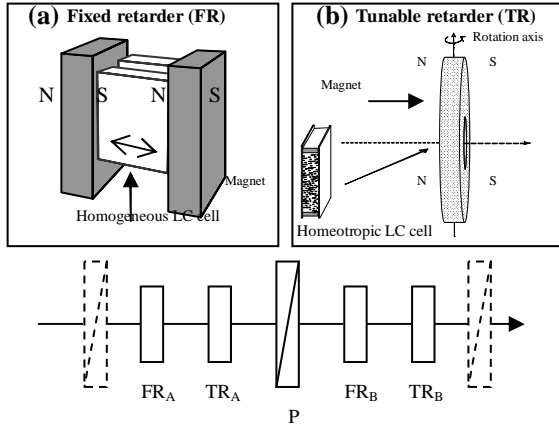

Fig. 10 The schematic diagram of the LC-based tunable THz Lyot filter: P: polarizer; N: North pole; S: South pole.

The transmittance, T, of the two-element Lyot filter for normally incident THz wave can be written as[20]

$$T = \cos^2\left(\frac{\Gamma_A + \Delta\Gamma_A}{2}\right) \cdot \cos^2\left(\frac{\Gamma_B + \Delta\Gamma_B}{2}\right). \tag{9}$$

Because of the birefringence of LC, the THz waves that pass through each element will be separated into extraordinary and ordinary rays (e-ray and o-ray) with corresponding time delays between the e-ray and o-ray, $\Delta\tau_A$ and $\Delta\tau_B$. The transmittance of the THz Lyot filter as a function of frequency of the THz waves, f, is given by

$$T(f) = \cos^2(\pi \cdot \Delta\tau_A \cdot f) \cdot \cos^2(\pi \cdot \Delta\tau_B \cdot f). \tag{10}$$

This Lyot filter is designed such that $\Delta\tau_B = 2\Delta\tau_A$. Satisfying this condition, $T(f)$ in Eq. (9) becomes

$$T(f) = 4\left(\cos^6(\pi \cdot \Delta\tau_A \cdot f) - \cos^4(\pi \cdot \Delta\tau_A \cdot f)\right) + \cos^2(\pi.\Delta\tau_A.f). \tag{11}$$

The first maxima of T(f) occur when the condition $\Delta\tau_A \cdot f = 1$ is fulfilled. The thicknesses of homogeneous LC layer in FR_A and FR_B, are 4.5 and 9 mm each. The thickness of LC layers in homeotropic cells for TR_A and TR_B, are 2 and 4 mm, respectively. The retardation of THz waves transmitted through the homeotropic cells can be tuned by rotating the magnets. The retardation provided by homeotropic cells, TR_A and TR_B will be zero when the LC molecules are parallel to the propagating direction of THz waves and increase with the reorientation of the LC molecules by rotating magnets. The filter was characterized by using a photoconductive-antenna-based THz time-domain spectrometer. The polarization of incident THz waves is parallel to the direction of the polarizer in the filter. The measurements are done around room temperature (~25ºC).

An example of the transmitted THz spectrum through the filter, normalized to the maximum of transmittance, is shown in Fig. 11. The transmitted peak frequency and the band width of the filter are 0.465 THz and ~0.10 THz, respectively. The theoretical curve according to Eq. (11), is shown as the solid curve, which is in good agreement with the experimental data. The corresponding THz temporal profile with total retardance, $\Delta\Gamma = 0$ is shown in the inset of Fig. 7. Note that there are four peaks with peak-to-peak separations of $\Delta\tau_A$. This can be understood as follows: The THz wave is separated into o-ray and e-ray after passing the first element and these two waves are further separated into o-o-ray, e-o-ray, o-e-ray and e-e-ray, respectively, again after passing the second element. The transmission spectrum manifests the interference among the four peaks of the THz signal.
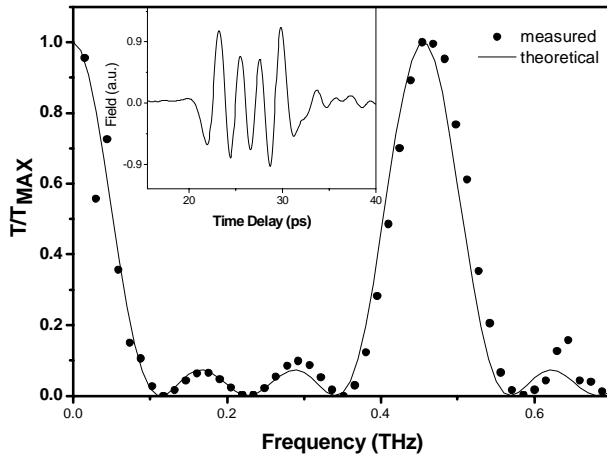

Fig. 11 An example of the transmitted spectrum of the broadband THz pulse through the LC THz Lyot filter, obtained by taking the FFT of the time-domain transmitted THz signal, which is shown in the inset.

The filter is tuned by rotating the magnets in TR_A and TR_B synchronously such that the condition $\Delta\tau_B=2\Delta\tau_A$ remains satisfied. To ensure fulfilling of this criterion, the dependence of $\Delta\tau_B$ and $\Delta\tau_A$ on rotation of the magnets are calibrated independently. The temporal THz profile is split from one peak into four peaks after passing through the two elements of the filter. The equal time difference, $\Delta\tau_A$, between each peak can be observed from measured data. The frequency dependent transmitted spectrum comes from the interference of these four parts of the THz signal and is obtained by applying FFT to the temporal signals. The peak transmission frequency of the filter decreases with the increasing $\Delta\tau_A$. The tuning range of the filter is from 0.388 to 0.564 THz or a fractional tuning range of ~ 40%.

CONTROL OF THz TRANSMISSION THROUGH TWO-DIMENSIONAL METALLIC PHOTONIC CRYSTALS USING LIQUID CYRSTALS

Metal films with two-dimensional periodic arrays (2D-MHA) or metallic photonic crystals (2D-MPC), can exhibit extraordinary optical transmission characteristics.[21] Enhanced THz emissions through 2D-MPC were recently reported.[22] This development could lead to the realization of ultra-sensitive THz sensing and imaging systems. Control of THz emission through 2D-MHA is also expected to add new functionalities to future THz photonic crystal devices. For a perfect metal, the transmission spectrum of the 2D-MHA with a triangular lattice of circular holes in the far-infrared is mainly characterized by several characteristic frequencies; the cutoff frequency of the TE_{11} mode, $v_c = 1.841c/\pi d$, where c is the speed of light in the holes and d is the diameter of the hole; the diffraction frequency, $v_{diff} = 2c'/\sqrt{3}$ s, where c' is the speed of light in the medium adjacent to the metal surface, s is the lattice constant; and the resonant frequency of the SPP on a structured surface due to coupling of between electromagnetic radiation incident on a grating and the SPP:[23]

$$v_R = v_{spp} = \left| \vec{k}_{in} + \vec{G} \right| \frac{c_o}{2\pi} \sqrt{\frac{\varepsilon_m + \varepsilon_d}{\varepsilon_m \varepsilon_d}} \ , \tag{12}$$

where $\vec{k}_{in}$ is the in-plane wave vector component of the incident THz wave, c_o is the speed of light in vacuum, $\vec{G}$ is the reciprocal lattice vectors of the periodic structure, ε_m and ε_d are the dielectric constants of the metal and the adjacent dielectric medium, respectively; v_c determines the lower frequency limit below which electromagnetic waves become evanescent in the metallic circular hole. The diffraction frequency determines the lowest frequency above which electromagnetic waves are diffracted into the first diffraction lobe. The transmission peak frequency of the 2D-MHA almost coincides with the resonant frequency of the SPP on a smooth surface. For THz waves propagating through the 2D-MHA, $|\varepsilon_m| >> \varepsilon_d$, the peak or resonant transmission frequency of the 2D-MHA,

$$v_R = v_{spp} \cong \frac{v_{diff}}{n_d} \ , \tag{13}$$

where v_{spp} is the surface plasmon-polariton (SPP) resonance frequency in the absence of the dielectric and $n_d = \sqrt{\varepsilon_d}$, where n_d is the index of refraction of the dielectric. It is then possible to tune the SPP resonance frequency monotonically by varying n_d. Recently, we have demonstrated frequency tuning of enhanced THz radiation transmitted through a 2D-MHA by controlling the index of refraction of 5CB filling the holes and adjacent to the 2D-MHA on one side.[24]

The 2D-MHA was a 0.5 mm-thick aluminum plate perforated with circular holes arrayed in a triangular lattice of lattice constant s = 0.99 mm and the diameter of each hole, d = 0.56 mm. The 2D-MHA was machined on the one side and sandwiched by a pair of Mylar sheets (75 μm in thickness) so that a box-like structure of dimension, $0.15 \times 15.0 \times 15.0$ mm^3, in the center of the 2D-MHA is formed for holding the LC (5CB, Aldrich, 98% purity). The holes of the MHA are also filled with LC material. A pair of rotatable permanent magnets is used to align the LC molecules as shown in Fig. 12. The magnetic field at the center on the sample cell is 0.15 T, which is much larger than the critical field (~0.05 T) required for aligning the LC molecules to the field. The LC cell is otherwise not aligned by any other means. By rotating the magnet assembly about the z-axis at an angle θ with respect to the sample plane (yz-plane in Fig. 1), the effective refractive index, n_d , of the LC infiltrated in and on one side of the 2D-MHA is changed from extra-ordinary refractive index, $n_e = 1.75$ to ordinary refractive index, $n_o = 1.57$. Since the magnetic field is significantly larger than the threshold field to re-orient the LC molecules, the effective refractive index of LC can be written as

$$n_d = \left\{ \left[\frac{\sin^2(\theta)}{n_o^2} + \frac{\cos^2(\theta)}{n_e^2} \right]^{-\frac{1}{2}} \right\} ,$$
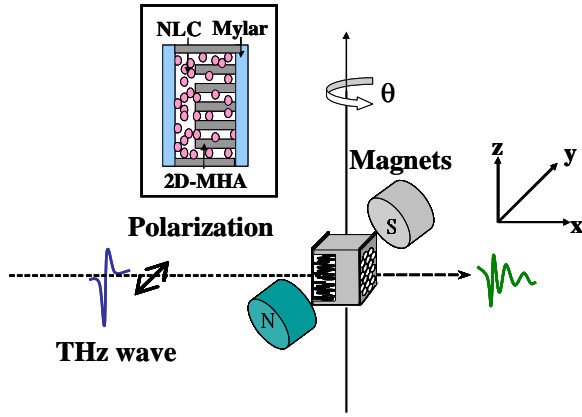
(14)

Fig.12 Experimental setup. The inset shows construction of the 2D-MHA with a nematic

By rotating the magnet assembly while keeping the sample stationary, we only change n_d without affecting the polarization direction of the THz wave. The maximum magnetic inclination angle is 55º. Beyond that, the THz beam would be blocked by the magnet in the current experimental setup. Spectral transmittance of the 2D-MHA is measured by using a photoconductive-antenna-based THz time-domain spectrometer (THz-TDS). The size of the 2D-MHA (about 250 holes in the aperture) is large enough to avoid the finite size effect. The finite time extent of the terahertz pulse scans, 136 ps (in 1024 steps), limits the frequency resolution of the numerical Fourier transforms in THz-TDS. To perform a numerical interpolation between the measured frequency points, the measured pulses in the time domain were extended with zeros (zero padding) to a total time duration of 1500 ps.

Figure 13 shows the measured zeroth-order transmission spectra for the 2D-MHA in several configurations.
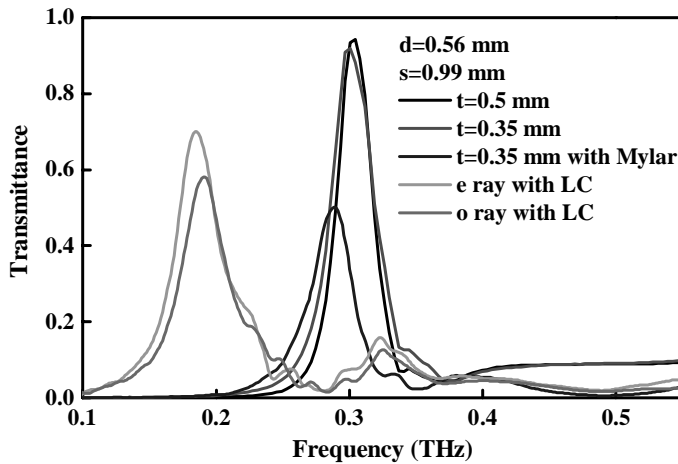

Fig. 13 Transmittance of the 2D-MHA sample before machining (thickness t = 0.5 mm, black trace), after machining into a box-line structure (t = 0.35 mm, red trace), boxed MHA with front and back Mylar sheets attached (blue trace), LC-filled MHA for o-ray (purple trace) and LC-filled MHA for e-ray (green trace).

The band-pass transmission peak for the 2D-MHA sample before machining (black trace) is observed at 0.304 THz. The peak transmission is close to unity, which is about 3 times higher than the value 0.29 expected from the porosity of the 2D-MHA. This transmission peak frequency is close to the resonant frequency of the SPP (0.349 THz) on a smooth surface and does not change appreciably after it was machined into the box-like structure (red trace). With front and back Mylar (n = 1.70, independently measured in our lab) sheets attached (blue trace), the peak frequency red-shifted to 0.289THz, while the cutoff behavior remains unchanged. The peak transmittance also reduces appreciably from 0.92 to 0.50. In this case, the peak frequency of the 2D-MHA is located below the cutoff frequency. As a result, the extinction coefficient of the waveguide mode becomes large as the resonant frequency of the SPP shifts to the lower frequency due to

the dielectric substrate while ν_c remains unchanged. Consequently the peak transmittance significantly decreases. The other possible mechanism is the decrease of the resonance effect between the SPP on the two sides of the metal slab, dielectric and air.

The frequencies of the main transmission peaks of LC-filled 2D-MHA for o-ray ($\vec{B} // \hat{z}$, purple trace in Fig. 12) and e-ray ($\vec{B} // \hat{y}$, green trace in Fig. 12), i.e., 5CB aligned perpendicular and parallel to the polarization of the incident THz wave, respectively, are red-shifted further to 0.193 THz and 0.188 THz. Using the indices of refraction of 5CB (n_o =

1.57 and $n_e = 1.75$) and expressions for the cutoff and diffraction frequencies presented earlier, we estimate that $\nu_c = 0.200$, $\nu_{diff} = 0.222$ and $\nu_R = 0.191$ THz for the perpendicular geometry (o-ray). Similarly, $\nu_c = 0.179$ THz, $\nu_{diff} = 0.199$ THz and $\nu_R = 0.171$ THz for the parallel geometry (e-ray). Thus the observed peak transmission frequencies are close to that of the theoretical estimates.

As we change from the perpendicular (o-ray) to the parallel (e-ray) geometry, the peak transmission (see Fig. 13) increases from 0.58 to 0.70. As a THz wave filter, the insertion loss of the present device is thus 2.35 to 1.55 dB, while the quality factors or Q-factors are between 4 and 5. For both geometries, the transmittance is larger than that of the device before filling with LC, 0.50. This can be qualitatively understood by noting that, while the resonance frequencies of the MHA-LC structures red-shifted to 0.191-0.171 THz, the cutoff frequency also shifted to a lower frequency of 0.2-0.179 THz from 0.314 THz for the bare 2D-MHA because a dielectric, LC is filled in the holes. Considering the porosity of the tunable 2D-MHA, 0.29, we observe an enhancement factor of 2.42.

We also plotted experimentally observed shifts of the peak transmission frequencies from those of the Mylar-packaged and boxed 2D-MHA before filling with LC as a function of the inverse of the effective index of refraction, $1/n_d$, in Fig. 14.
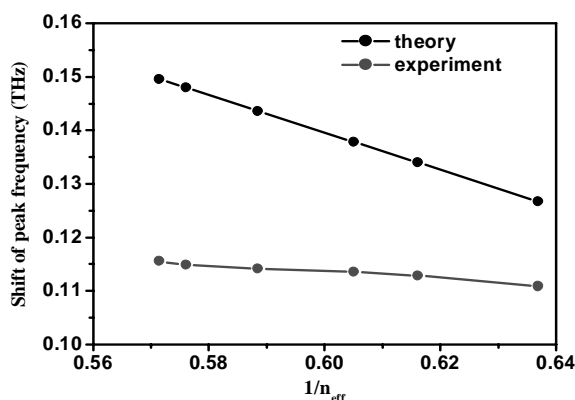

Fig. 14 The experimentally observed shift of the peak frequencies from Fig. 13 and the theoretical estimates are plotted as a function of the inverse of the effective index of refraction.

The experimentally obtained tuning range is 0.0047 THz as we vary θ from 0° to 90°. An estimate of the potential tuning range of the device can be deduced from Eq. (2), $|\Delta\nu_R| \sim \Delta n_d \nu_{spp}/n_d^2$, where ν_{spp} is the resonance frequency of the device before filling with LC. For the ideal case, if the substrate is infinite, the maximun tuning range using 5CB should then be ~ 0.02 THz. It has previously shown that the frequency shift can be increased by using matching dielectric substrates on both side of the 2D-MHA. This is expected to be the case for the current device with LC also.

The shifts according to the theoretical estimates using Eq. (13), $|\nu_R - \nu_{diff}| = \nu_{diff}|(1/n_d)-1|$, are also shown in the same figure. General linear trends with $1/n_d$ are observed for both. There is, however, significant discrepancy in the slopes of the two. Qualitatively, this can be understood by noting that the theoretical model assumes an infinite dielectric substrate. Experimentally, the liquid crystal "substrate" is of finite thickness. Further, Eq. (12) does not take into account effect of filling of the holes with LC instead of air. It could be argued that it is not necessary to invoke SPPs in order to explain the measurements, as the cutoff frequency also varies with the index of refraction of the LC in the holes. The transmission peak frequency, however, does not necessarily change with the cut-off frequency. We have measured the zero-order transmission spectra of the 2D-MHA by changing the thickness of the dielectric (polymer) layer and found that the band-pass transmission peak shifts to the lower frequency side with increasing the layer thickness, even though the cutoff frequency does not change (the material filling the holes were air always in that experiment). We note that the error in the measurement of the peak positions is ~ 0.0007 THz, much smaller than the shift we detected, 0.0047 THz. Because the SPP resonance frequencies and the cutoff frequencies are very close in the present experiment, however, we cannot rule out completely the possibility that the peaks could be guided modes in the holes.

The change in peak transmittance of the 2D-MHA by varying the effective index of refraction of the LC is shown in Fig. 15. The THz transmission peak increases with θ for $\theta < 30°$. This can be explained by how close the refractive index of LC matches that of Mylar. The ordinary and extraordinary refractive indices of 5CB are 1.57 and 1.75, respectively, at 0.3 THz. With increasing θ, the effective refractive index of LC will descend from 1.75 to 1.70 (from θ

= 0° to $\theta = 30°$) and the refractive index of Mylar substrate, which is 1.70. Over 30°, n_d will decrease from 1.70 to 1.57 with increasing θ. The transmission peak will then decrease according to the same theory.
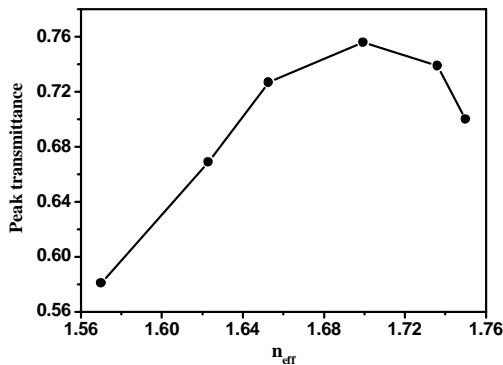

Fig.15 The peak transmittance of the 2D-MHA is plotted as a function of the inverse of the effective index of refraction of the

In summary, we demonstrate frequency tuning of enhanced THz radiation transmitted through a two-dimensional metallic hole array (2D-MHA) by controlling the index of refraction of the medium filling the holes and adjacent to the 2D-MHA on one side. The medium is a nematic liquid crystal (NLC) 5CB and its index of refraction is varied using the dependence of the effective index of refraction of the NLC on the magnetic field. With the NLC, the peak transmission frequency of the 2D-MHA shifts to the red by 0.112 THz and can be tuned between 0.193 and 0.188 THz. The maximum transmission of the device is well above (2.42 times) that according to the fractional area occupied by the holes and varies from 55% to above 70%. As a filter, the present device exhibits a continuous tuning range of 4.5 GHz, relatively low insertion losses of 2.35 to 1.55 dB and a Q-factor of ~ 4-5. The tuning range can be as high as 0.037 THz by employing matching LC substrates on both sides of the 2D-MHA and highly anisotropic LC materials. The Q-factor can be improved by cascading two or more such filters.

SUMMARY

We present recent progress in liquid crystal THz optics from our group. Using time-domain THz spectroscopy, we have determined the complex indices of refraction of nematic liquid crystals, 5CB, PCH5 and E7 from 0.2 to beyond 1 THz. Significantly, the birefringence of 5CB and E7 are found to be as large as 0.2 at THz frequencies, while the absorption is negligible. Electrical-field and magnetic-field-controlled birefringence in LC were also investigated. A tunable room-temperature THz phase shifter using magnetic-field-controlled birefringence in nematic 5CB gives a phase shift as large as 108° at 1.0 THz. Phase shift exceeding 360° at 1 THz, an important milestone, was realized by using a sandwiched LC (E7, Merck) cell as thick as 3 mm. An electrically-tuned LC THz phase shifter capable of more than 90° of phase shift and operation of the device as a quarter-wave plate at 1 THz was also demonstrated. The magnetically tuned LC phase shifter served as key components in a two-element tunable LC Lyot filter. The tuning range of the filter is from 0.388 to 0.564 THz or a fractional tuning range of ~ 40%. Our work clearly demonstrates the potential of liquid crystal devices for THz applications. Finally, we will present initial works on control of enhanced THz transmission through a metallic hole array with nematic liquid crystals. Our work clearly demonstrates the potential of liquid crystal devices for THz applications.

ACKNOWLEDGEMENTS

REFERENCES

1.   D. Mittleman, "Terahertz Imaging," in Sensing with THz radiation, (Spring-Verlag, New York, 2002).

2. Peter H. Siegel," Terahertz technology," IEEE Trans. Microwave Theory Tech. **50**, 910-928 (2002).
3. B. Ferguson and X.-C. Zhang," Materials for terahertz science and technology," Nature Materials, **1**, 26-33 (2002).
4. E. G.Hanson, and Y. R. Shen, "Refractive indices and optical anisotropy of homologous liquid crystals," Mol. Cryst. Liq. Cryst. **36**, 193-207 (1976).
5. E. Miraldi, C. Oldano, L.Trossi, and P. T. Valabrega, "Direct measurement of the two refractive indexes of a nematic liquid crystal slab," Appl. Opt. **21**, 4163-4166 (1982).
6. S. T. Wu, U. Efron, and L. V. Hess, "Infrared birefringence of liquid crystals," Appl. Phys. Lett. **44**, 1033-1035 (1984).
7. K. C. Lim, J. D. Margerum, A. M. Lackner, L. J. Miller, E. Sherman, and W. H. Smith, "Liquid crystal birefringence for millimeter wave radar," Liq. Cryst. **14**, 327-337 (1993).
8. T. Nose, S. Sato, K. Mizuno, J. Bae, and T. Nozokido, "Refractive index of nematic liquid crystals in the submillimeter wave region" Appl. Opt. **36**, 6383-6387 (1997).
9. D. Turchinovich, P. Knobloch, G. Luessem, and M. Koch, "THz Time-Domain Spectroscopy on 4-(trans-4'-pentylcyclohexyl)-benzonitril," in Liquid Crystal V, I. C. Khoo, ed., Proc. SPIE **4463**, 9-14 (2001).
10. T. R. Tsai, C.-Y. Chen, C. –L. Pan, R.-P. Pan, and X.-C. Zhang, "THz Time-Domain Spectroscopy Studies of the Optical Constants of the Nematic Liquid Crystal 5CB", Appl. Optics **42,** 2372-2376 (2003).
11. R.-P. Pan, T. –R. Tsai, C. –Y. Chen, and C.-L. Pan, "Optical Constants of Two Typical Liquid Crystals 5CB and PCH5 in the THz Frequency Range", J. of Biological Physics **29**, 335-338 (2003).
12. Tze-An Liu, Masahiko Tani, and Ci-Ling Pan , J. Appl. Phys. **93**, 2996 (2003).
13. Chao-Yuan Chen, Tsong-Ru Tsai, Ci-Ling Pan, and Ru-Pin Pan"Terahertz Phase Shifter with Nematic Liquid Crystal in a Magnetic Field", Appl. Phy. Letts. **83**, 4497-4499 (2003).
14. Chao-Yuan Chen, Cho-Fan Hsieh, Yea-Feng Lin, Ru-Pin Pan, and Ci-Ling Pan, "Magnetically Tunable Room-Temperature 2π Liquid Crystal Terahertz Phase Shifter," Opt. Express **12**, 2625-2630 (2004).
15. T.-R. Tsai, C.-Y. Chen, R.-P. Pan, C.-L. Pan, and X.-C. Zhang, "Room Temperature Electrically Controlled Terahertz Phase Shifter," IEEE Microwave Wireless Comp. Lett. **14**, 77-79 (2004).
16. P. G. de Gennes and J. Prost, The Physics of Liquid Crystals, 2nd ed. (Oxford, New York, 1983).
17. S. Chandrasekhar, Liquid Crystal, 2nd ed. (Cambridge, New York, 1992).
18. K. Skarp, S. T. Lagerwall, and B. Stebler, "Measurements of hydrodynamic parameters for 5CB," Mol. Cryst. Liq. Cryst. **60**, 215-236 (1980).
19. B. Lyot, "Un monochromateur grand champ utilisant les interferences en lumiere polarisee, » Ann. Astrophys., **7**, 1593-1595 (1944).
20. Chao-Yuan Chen, Cho-Fan Hsieh, Yea-Feng Lin, Ci-Ling Pan and Ru-Pin Pan, "A Liquid-Crystal-Based Terahertz Tunable Lyot Filter," to be published in Appl. Phys. Lett., 2006.
21. T. W. Ebbesen, H. J. Lezec, H. F. Ghaemi, T. Thio, and P. A. Wolff, "Extraordinary optical transmission through sub-wavelength hole arrays," Nature (London) **351**, 667 (1998).
22. F. Miyamaru and M. Hangyo, "Anomalous terahertz transmission through double-layer metal hole arrays by coupling of surface plasmon polaritons," Phys. Rev. B**71**, 165408 (2005).
23. H. F. Ghaemi, T. Thio, D. E. Grupp, T. W. Ebbesen, and H. J. Lezec, "Surface plasmons enhance optical transmission through subwavelength holes," Phys. Rev. B **58**, 6779 (1998).
24. Ci-Ling Pan, Cho-Fan Hsieh, and Ru-Pin Pan, Masaki Tanaka, Fumiaki Miyamaru, Masahiko Tani, and Masanori Hangyo, "Control of enhanced THz transmission through metallic hole arrays using nematic liquid crystal," Optics Express **13**, 3921 – 3930 (2005).